Journal of Power Sources 209 (2012) 1–6

Contents lists available at SciVerse ScienceDirect

Journal of Power Sources

journal homepage: www.elsevier.com/locate/jpowsour

Graphene anchored with nickel nanoparticles as a high-performance anode material for lithium ion batteries

Y.J. Mai, J.P. Tu*, C.D. Gu, X.L. Wang

State Key Laboratory of Silicon Materials and Department of Materials Science and Engineering, Zhejiang University, Hangzhou 310027, China

ARTICLE INFO

Article history:
Received 10 August 2011
Received in revised form 17 February 2012
Accepted 20 February 2012
Available online 28 February 2012

Keywords:
Graphene
Nickel nanoparticles
Anode
Lithium ion battery

ABSTRACT

The surface of graphene is modified by nickel nanoparticles which are in-situ reduced from NiO nanoparticles by graphene. The nickel nanoparticles obtained are up to 10 nm in size and are strongly anchored on the surface of graphene sheets. As an anode material for lithium ion batteries, the graphene–Ni hybrid material delivers a reversible capacity of 675 mAh g^{-1} after 35 discharge/charge cycles at a current density of 100 mA g^{-1}, corresponding to 85% retention of the initial charge capacity. In addition, the graphene–Ni hybrid electrode exhibits much better rate capability compared to its pure counterpart operated at various rates between 200 and 800 mA g^{-1}. Such enhanced lithium storage performance of the graphene–Ni hybrid electrode can be ascribed to the enhanced electronic transport and Li^+ migration through the solid electrolyte interphase (SEI) film as a consequence of that the anchored nickel nanoparticles increase the electronic conductivity and modify the structure of SEI film covering the surface of graphene.

1. Introduction

Lithium ion batteries (LIBs) currently dominate the market of various portable electronics as power sources. Their performance of charge/discharge urgently needs to be improved to satisfy the high power and/or energy densities applications such as electrical/hybrid vehicles and miscellaneous power devices. Generally, in order to achieve high power, high energy and long life, rapid ionic and electronic transport in stable electrode materials is necessary [1–6].

Graphene, the mother of all graphitic forms, is considered as a promising anode material, due to its superior electrical conductivity, high surface-to-volume ratio and abundance of raw materials. Especially, it offers a prospect for increasing the energy density of batteries because the lithium could be accommodated not only at the next neighboring sites of stage 1 graphite intercalation compounds, except the regular sites of LiC_6 [7], but also on the edges and other defects of graphene sheets [8]. Unfortunately, according to the recent reports, bare graphene displayed a small reversible specific capacity at a relatively high current density and poor rate performance [7–13]. For example, when the current density was 200 mA g^{-1}, the bare graphene electrode displayed a capacity of about 250 mAh g^{-1} after 40 cycles and even at a current density of 50 mA g^{-1}, the pure graphene only delivered a capacity of 290 mAh g^{-1} after 20 cycles [11]. However, its reversible specific capacity was increased up to 730 and 780 mAh g^{-1}, respectively, by the incorporation of carbon nanotubes and fullerenes to the graphene [7]. So, it seems that additional decoration is necessary in order to increase its lithium storage performance. It is well known that the electronic transport in electrode materials can be greatly improved by the conductive additives [14–16]. Also, chemical modifications of the graphite electrode surface are demonstrated to be useful in enhancing the kinetics of lithium intercalation because they can optimize the formation of the solid electrolyte interphase (SEI) and all lithium ions in an electrolyte solution must cross this surface film before the formation of the lithium-intercalation graphite compounds [17–20].

In this present work, the surface of graphene is modified by introducing nickel nanoparticles, which are in situ reduced from NiO nanoparticles by the graphene. When the nickel-modified graphene is used as an anode material of LIBs, it shows a larger reversible capacity and better rate performance compared to the bare graphene electrode. Although these anchored nickel nanoparticles do not directly contribute to the capacity, they accelerate charge transfer and Li^+ diffusion across the surface film, reducing the polarization of the host material. Different from previous reports on metal oxide/alloy nanoparticles encapsulated by graphene sheets with a high specific capacity and excellent cycling performance as anode materials in LIBs, in which the graphene acts as both the buffer zone of volume variation of the nanoparticles and the good electron transfer medium [10,13,21–25], the present nickel-modified graphene hybrid material highlights that the nanosheet form of graphene is a promising anode material after appropriate modification.

* Corresponding author. Tel.: +86 571 87952856; fax: +86 571 87952573.
E-mail addresses: tujp@zju.edu.cn, tujplab@zju.edu.cn (J.P. Tu).

0378-7753/$ – see front matter © 2012 Elsevier B.V. All rights reserved.
doi:10.1016/j.jpowsour.2012.02.073

2. Experimental

For the sake of brevity, the nickel-modified graphene is denoted as the graphene–Ni hybrid material. This material was prepared as follows. First of all, 270 mg graphene oxide (GO) obtained by a modification of Hummers' method with graphite flakes as the starting material [26], was dispersed in 540 ml de-ion water by sonication for 30 min. An appropriate amount of $Ni(NO_3)_2{\cdot}6H_2O$ (Sinopharm Chemical Reagent Co., Ltd.), followed by ammonia solution (0.55 M) was slowly added into the above suspension and then stirred for 2 h at room temperature. The obtained precursor, i.e. GO–$Ni(OH)_2$ hybrid material, was collected by freezing drying and then calcined in a tube furnace at 500 °C for 2 h in flowing argon. For comparison, pure graphene was reduced from GO under the same thermal reduction condition.

The graphene–Ni hybrid material was characterized by means of X-ray diffraction (XRD, D/max 2550-PC), X-ray photoelectron spectroscopy (XPS, AXIS UTLTRADLD) and transmission electron microscopy (TEM, CM200 and Tecnai F30). Thermogravimetry (TG, SDT Q600 V8.2 Build 100) analysis from room temperature to 700 °C at a heating rate of 10 °C min^{-1} in air was carried out to estimate the weight percentage of nickel in the hybrid material.

The working electrodes were prepared by a slurry coating procedure. The slurry consisting of 90 wt.% the as-synthesized powder (graphene–Ni hybrid material, pure graphene) and 10 wt.% polyvinylidene fluorides dissolved in *N*-methyl pyrrolidinone (Sinopharm Chemical Reagent Co., Ltd.) was incorporated on nickel foam with 15 mm in diameter. The electrolyte (Guotai-Huarong New Chemical Materials Co., Ltd) was 1 M $LiPF_6$ in ethylene carbonate–dimethyl carbonate (1:1 v/v). CR-2025-type coin cells were assembled in a glove box under argon atmosphere. The galvanostatic discharge/charge measurements were conducted on LAND battery program-control test system between 0.02 and 3.0 V. The theoretical capacity of graphene sheets is not sure so far, so it is difficult to define the *C* rate and the specific current density in the form of milliampere per gram is used in this work. The electrochemical impedance spectroscopy (EIS) measurements were carried out in a three-electrode cell in the frequency range from 0.01 Hz to 100 kHz on a CHI660 C electrochemical workstation and the impedance data were fitted using the ZsimpWin computer program. Before the EIS measurement, the cells were cycled for 10 cycles at a current density of 50 mA g^{-1}, then discharged to 2.5 V (versus Li/Li^+) and kept until the open-circuit voltage stabilized. All the tests were conducted at room temperature (25 ± 1 °C).

3. Results and discussion

Fig. 1a shows the XRD patterns of the as-prepared materials calcined at 300 and 500 °C. These patterns indicate the formation mechanism of the graphene–Ni hybrid materials. First of all, $Ni(OH)_2$ nanoparticles are obtained by the reaction between $Ni(NO_3)_2$ and NH_3 H_2O [27]. It is reasonable to think that the $Ni(OH)_2$ nanoparticles nucleate and grow on the surface of GO sheets as a form of heterogeneous nucleation, especially at the defect sites and the edge plane. After calcining at 300 °C, $Ni(OH)_2$ nanoparticles dehydrate to NiO nanoparticles, and GO is reduced to graphene. With further increasing the temperature up to 500 °C, NiO nanoparticles are reduced to nickel nanoparticles by the graphene. The broad nature of (0 0 2) diffraction peak of graphene indicates poor ordering of the sheets along the stacking direction, implying that the graphene is mostly composed of a few layers, which are consistent with the TEM results (the following section). Also, the other diffraction peaks owing to NiO or metallic nickel broaden obviously, indicating the nature of nanoparticles. It is hypothesized that the only remain is NiO (11.8 wt.%, as shown in the result of TG in Fig. 1b) after the calcination of the graphene–Ni hybrid material at 700 °C in air because the nickel nanoparticles in the hybrid materials undergo the oxidation process. So the weight percentage of nickel in the hybrid material is estimated to be 9.5 wt.%.

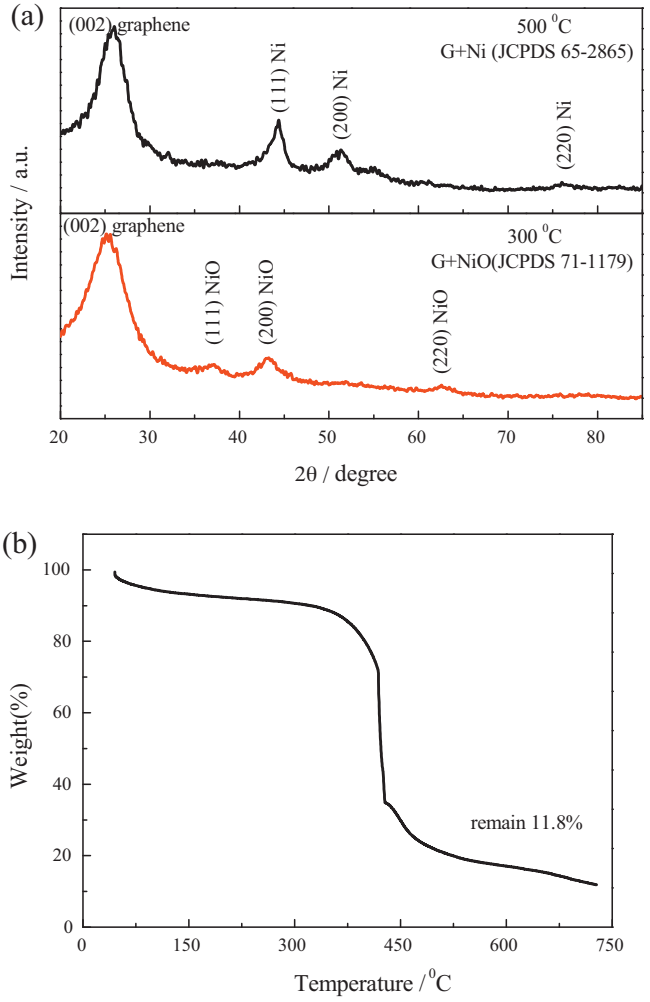

Fig. 1. (a) XRD patterns of the as-prepared materials, (b) TG curve of the graphene–Ni hybrid material, measured from room temperature to 700 °C at a heating rate of 10 °C min^{-1} in air.

XPS analysis can be used to characterize the thermal reduced graphene. In Fig. 2a, three most prominent components are clearly seen in C1s region of GO, including the component of sp^2-C, corresponding to sp^2 hybridized carbon species, the component of C═O, corresponding to the carboxyl and the component of C—O, corresponding to hydroxyl and epoxy, which indicate the high degree oxidation of GO. As shown in Fig. 2b, however, after thermal reduction, most chemically attached functional groups are successfully removed and the portion of sp^2 hybridized carbon species obviously increases, which is in agreement with the previous reports [28,29].

Fig. 3a shows TEM images of the reduced GO, revealing the rippled and crumpled paper-like morphology. What is more, many shadows with weak gray color are observed, indicating uncontrolled reassembling of the graphene sheets during drying. The cross sectional TEM image is used to further characterize the stacking sheet structure. Some parts of the graphene sheets are wavy and turbostratic, suggesting that the layer stacking is no longer as ordering as graphite, but disordering [7]. Furthermore, as shown in Fig. 3b and c, the nickel nanoparticles obtained are up to 10 nm in

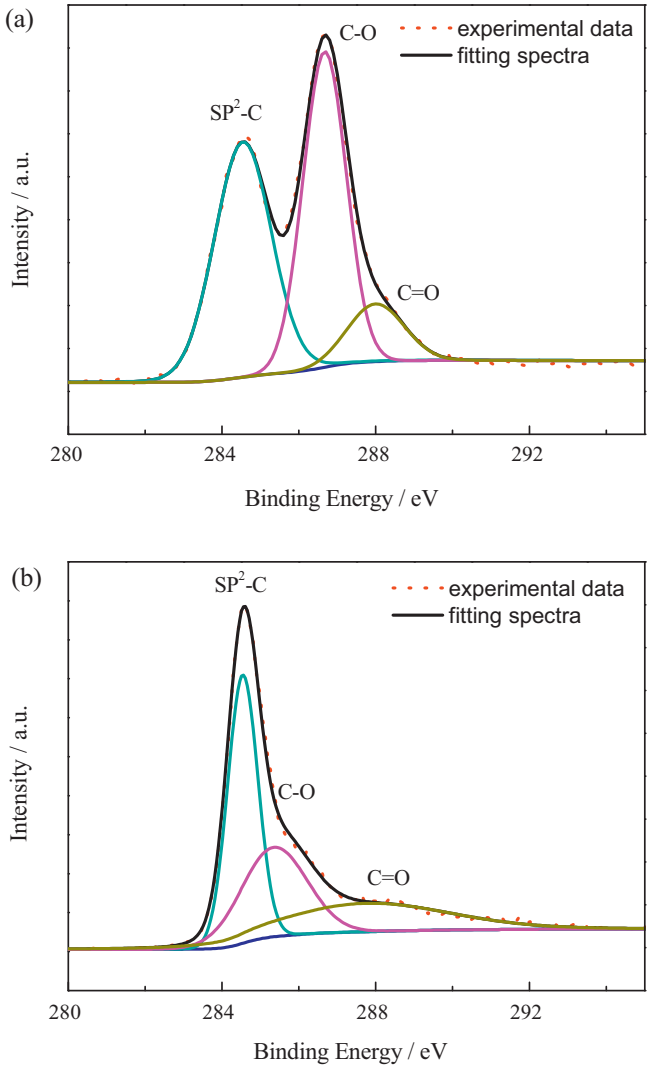

Fig. 2. XPS C1s spectra of (a) GO and (b) graphene–Ni hybrid material.

size and are strongly anchored on the surface of graphene sheets. Recently, defects of GO and graphene, which originate from the oxidation–reduction treatment, have been directly observed by atomic resolution TEM [30,31], and these defects prefer to afford active sites for the nucleation and growth of nanoparticles [32]. On the other hand, the defects of carbon materials are considered as the active sites for the formation of SEI film [33]. It is reported that chemical modification of graphite surface by metal oxide/metal [19,34], lithium carbonate [18,20] and coke/pyrolytic carbon coating [17,33] could obtain a moderate development of this film. Therefore, it is expected that the anchored nickel nanoparticles will optimize the development of SEI film and increase the electronic conductivity of the present graphene, which benefit the reversible capacity and rate performance when it is used as an anode material for LIBs.

Fig. 4 shows the discharge/charge profiles of pure graphene and graphene–Ni hybrid electrodes at a current density of 100 mA g^{-1}. The first discharge and charge capacities are 1013.2 and 550.7 mAh g^{-1} for the pure graphene, corresponding to an initial columbic efficiency of 54%, whereas, 1307.9 and 790 mAh g^{-1} for the graphene–Ni hybrid electrode, corresponding to an improved initial columbic efficiency of 60%. Two potential regions, characterized with different slopes, are observed in the discharge curves. They include the one lower than 0.5 V (vs. Li/Li^+)

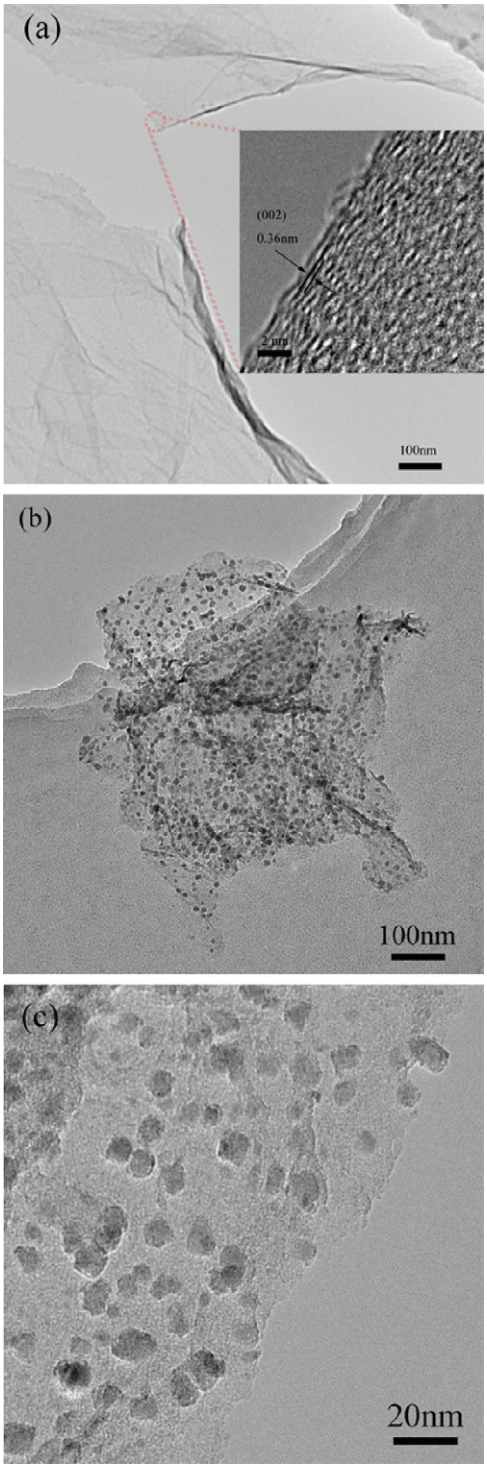

Fig. 3. TEM images of (a) thermal reduction graphene and the inset is the cross sectional TEM image, graphene–Ni hybrid material with low-magnification (b) and high-magnification (c).

corresponding to the lithium intercalation into the graphene sheets which are stacked in a roughly parallel fashion [35,36], and the other one from open circuit potential to 0.5 V, corresponding to a faradic capacitance. This faradic capacitance occurs either on the edge planes or the graphene surface containing vacancies and adsorbed functional groups [7–9,37,38]. It is noteworthy that there is something to worry about that the metallic impurities will act as nucleus for dendrite formation which will lead to cell shorting.

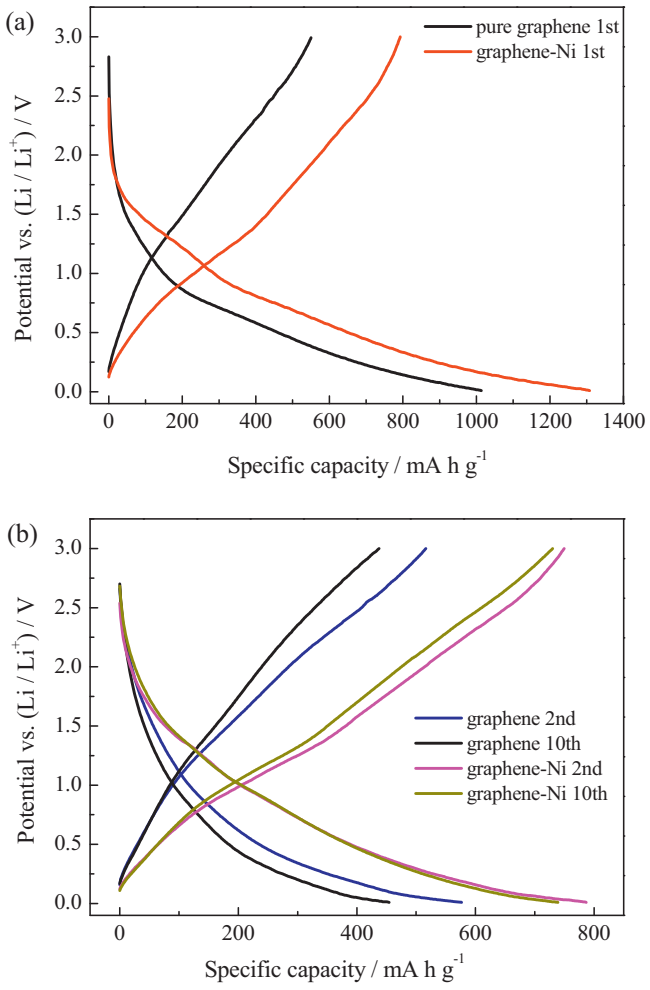

Fig. 4. Discharge/charge profiles of pure graphene and graphene–Ni hybrid electrodes: (a) the first cycle, (b) the second and the tenth cycle.

Indeed, the metallic lithium will be electrodeposited on the surface of carbon if the cell is discharged to an enough low potential. If the plating of lithium occurs, the cell voltage rises slightly even though the cell is still discharging because the overvoltage associated with plating of lithium is reduced once a significant amount of plated metal is formed [35]. However, the galvanostatic discharge profiles between 0.02 and 3.0 V at a current density of 100 mA g^{-1} does not show any rise of cell voltage (Fig. 4), even though the current density is as low as 18.6 mA g^{-1} (the date are not shown here), suggesting that no plating of lithium occurs. The phenomenon of plating-free of lithium was also observed for the copper deposited graphite electrode [34]. What is more, many Li/graphene–Ni half cells have successfully cycled at different current densities and no cell suffers from shorting. Thus, we think that the metallic particles will not promote the nucleation and growth of lithium dendrite in the present voltage range of 0.02–3.0 V. However, when the cell is discharged to an enough low voltage such as slightly below zero volts when the plating of lithium occurs, whether the metallic particles will act as nucleus to promote the dendrite formation or not is still unsure and further investigation is needed. Comparison on the discharge/charge profiles of both the electrodes indicates an obvious advantage of the hybrid material electrode which exhibits a reduced polarization during both intercalation and deintercalation of lithium, as shown in Fig. 4a, and this advantage still exists in the following cycles (Fig. 4b). It is believed that such reduced polarization benefits the reversible capacity and especially the rate performance.

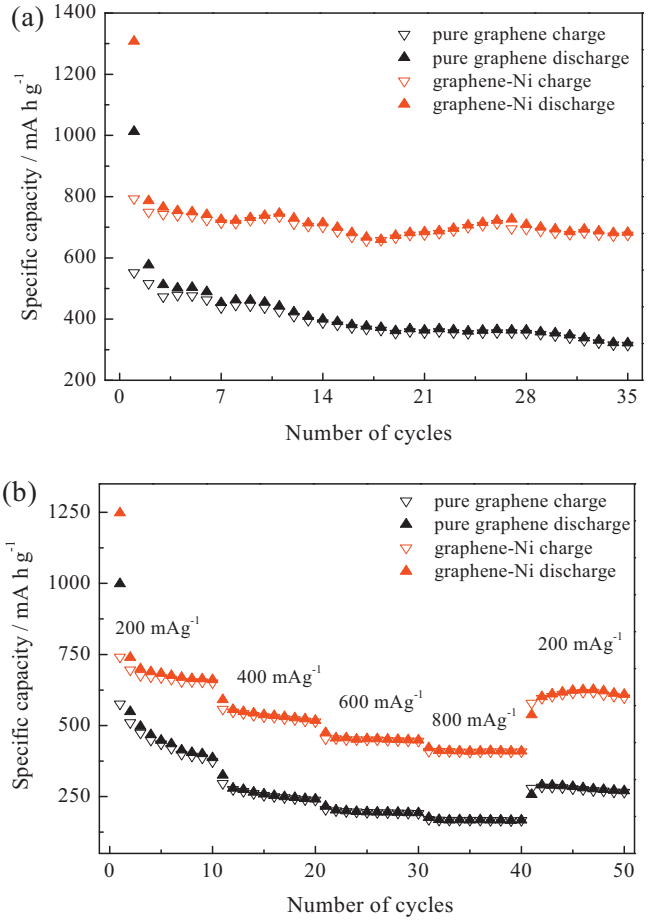

Fig. 5. (a) Cyclic performance at a current density of 100 mA g^{-1} and (b) rate performance of the pure graphene and graphene–Ni hybrid electrodes.

Indeed, the graphene–Ni hybrid electrode exhibits larger reversible capacity and better cyclic performance than the bare graphene electrode, as shown in Fig. 5a. At a current density of 100 mA g^{-1}, the pure graphene electrode shows a reversible capacity of 314.8 mAh g^{-1} after 35 cycles, just 57% of the initial charge capacity, which is consistent with previous reports [7,39–41]. For the graphene–Ni hybrid electrode, the reversible capacity retains 675 mAh g^{-1} after 35 cycles, which is 85% retention of the initial charge capacity. This reversible capacity is comparable to the 600 °C-pyrolytic GO prepared by Pan et al. [8], who reported that the enhanced capacity in disordered graphene could be ascribed to those additional storage sites such as edges and other defects. In addition, the graphene–Ni hybrid electrode exhibits much better rate capability compared to its pure counterpart operated at various rates between 200 and 800 mA g^{-1} (Fig. 5b). For example, in the case of hybrid material, the reversible capacity is stable at 660 mAh g^{-1} after 10 cycles at a current density of 200 mA g^{-1}. Upon increasing the discharge/charge current density to 400, 600 and 800 mA g^{-1}, its reversible capacity still maintains at 520, 450, and 410 mAh g^{-1}, respectively, which is remarkably better than that of the pure graphene electrode. These reversible capacities are comparable to the high quality graphene sheets reported by Wang and co-workers [12]. Furthermore, our hybrid material shows better cyclic performance at stepwise current densities.

To understand the reason for the improved electrochemical lithium storage performance of the graphene–Ni electrode, EIS measurements are carried out after the 10th cycle at a current density of 50 mA g^{-1}. The Nyquist plots of the pure graphene and the graphene–Ni hybrid electrodes are shown in Fig. 6a. Apparently,

Table 1
Typical parameters obtained by fitting an equivalent circuit of the pure graphene and graphene–Ni hybrid electrodes.

Electrode	R_{sf1} (()	R_{sf2} (()	R_{sf3} (()	R_{sf4} (()	R_{sf} (()	R_{ct} (()
Pure graphene	7.7 ± 0.6	30.9 ± 2	103.8 ± 2	4.7 ± 0.4	147.1 ± 5	30.1 ± 1.9
Graphene–Ni hybrid material	7.5 ± 0.8	3.1 ± 0.5	22.8 ± 3.1	3.2 ± 1.7	36.6 ± 6.1	17 ± 2.7

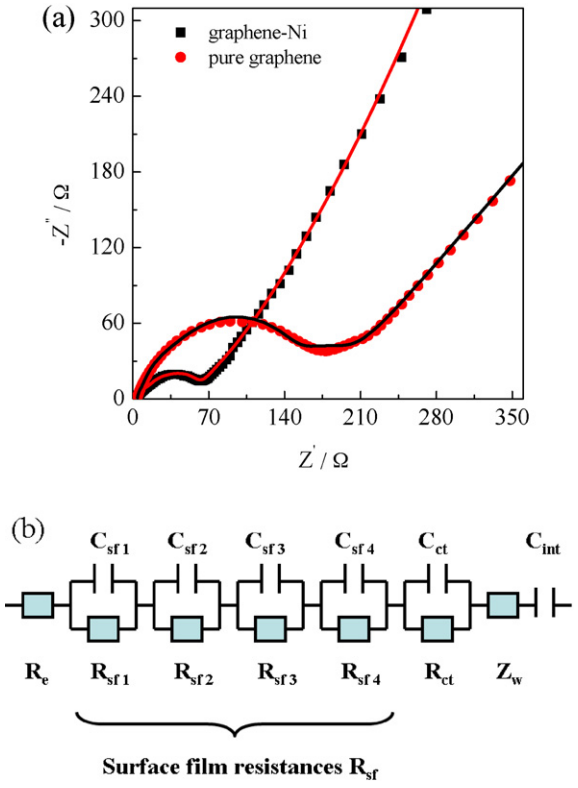

Fig. 6. (a) Nyquist plots (the symbols) and the fitted spectra (the continuous lines) of the pure graphene and the graphene–Ni hybrid electrodes, respectively, in the potential of 2.5 V (vs. Li/Li$^+$) after 10 discharge/charge cycles; (b) equivalent electrical circuit used to model.

the semicircle diameter of hybrid material electrode is rather small with respect to that of the pure graphene, indicating the smaller surface film resistance and lithium-ion charge transfer resistance. This assumption is further confirmed by fitting to an equivalent circuit as shown in Fig. 6b. Aurbach et al. [42] demonstrated by means of XPS that the SEI had a multilayer structure due to difference in their composition as a function of the distance of the surface species precipitated from the active reductive electrode surface. Thus, a "Voigt"-type equivalent analog of several $R||C$ circuits in series (R_{sfi} and C_{sfi}, i = 1, 2, 3, and 4) can be used to model the migration of Li$^+$ through such surface films with a multilayer structure, in which each of these $R||C$ circuits relates to Li$^+$ migration through one of the layers composing the surface films covering the surface of graphene [43]. R_e represents the electrolyte resistance and R_{ct} is the charge transfer resistance of lithium ions at the interface between electrolyte and electrode. W_s and C_{int} correspond to the solid state diffusion in graphene and intercalation capacitance, respectively [44–46]. In Fig. 6a, the symbols are the experimental data whereas the continuous lines represent the fitted spectra. Typical parameters are summarized in Table 1, revealing that the surface film resistance ($R_{sf} = \sum R_{sfi}$, i = 1, 2, 3 and 4) and R_{ct} for the pure graphene electrode are 147.1 ± 5 and 30.1 ± 1.9 (, respectively, whereas for the graphene–Ni hybrid electrode, they are drastically reduced to 36.6 ± 6.1 and 17 ± 2.7 (, respectively, suggesting the enhanced kinetics of Li$^+$ and electronic transport. For the insertion reaction electrodes, lithium ions are inserted into an open host structure with electron addition followed by an extraction of lithium ions with electron removal during cycling. Thus, their rate performance is limited by the Li$^+$ diffusion and electron transport in the electrode. Previous reports demonstrated that there are many defects on the surface of GO and graphene obtained by oxidation–reduction treatment [30,31], and these defects prefer to afford active sites for the nucleation and growth of nanoparticles [32]. So, it is reasonable to believe that the anchored nickel nanoparticles can cover and/or remove some active sites existing on the surface of graphene, which are favored for the formation of thicker SEI film. Thus, they are capable of optimizing the formation of SEI films. It is such a modified surface that enhances the kinetics of lithium intercalation because all lithium ions in an electrolyte solution must cross the SEI film before the formation of the lithium-intercalation graphite compounds. In addition, according to the previous reports [26,28,29], the conductivity of graphene obtained by oxidation-thermal reduction treatment is in a range from several up to several hundreds S cm^{-1} and is still far behind metallic nickel (1.46×10^5 S cm^{-1}), so it is expected that the nickel nanoparticles increase the electrical conductivity of the host material. The above two reasons are well accounted for the enhanced lithium storage performance of the graphene–Ni hybrid material.

4. Conclusions

The surface of graphene is modified by anchoring with nickel nanoparticles. Such a microstructure provides favorable transport kinetics for both the lithium ions diffusion across the SEI film and the electronic transfer. As a result, this graphene–Ni hybrid electrode delivers a reversible capacity of 675 mAh g^{-1} after 35 cycles at a current density of 100 mA g^{-1}, which is more than twice than that of the pure graphene electrode. And the retention after 35 cycles is 85% of the initial charge capacity. When the current density is increased to 800 mA g^{-1}, the hybrid electrode still exhibits a reversible capacity of 410 mAh g^{-1} and also good rate performance, highlighting that the nanosheet form of graphene is a promising anode material after appropriate modification.

References

[1] D.W. Liu, G.Z. Cao, Energy Environ. Sci. 3 (2010) 1218–1237.
[2] M.H. Liang, L.J. Zhi, J. Mater. Chem. 19 (2009) 5871–5878.
[3] X.H. Huang, J.P. Tu, Z.Y. Zeng, J.Y. Xiang, X.B. Zhao, J. Electrochem. Soc. 155 (2008) A438–A441.
[4] S.R. Gowda, A.L.M. Reddy, M.M. Shaijumon, X. Zhan, L. Ci, P.M. Ajayan, Nano Lett. 11 (2010) 101–106.
[5] X.H. Huang, J.P. Tu, X.H. Xia, J.Y. Xiang, X.L. Wang, J. Power Sources 195 (2010) 1207–1210.
[6] X.H. Xia, J.P. Tu, J.Y. Xiang, X.H. Huang, J. Zhang, X.L. Wang, X.B. Zhao, J. Power Sources 195 (2010) 2014–2022.
[7] E. Yoo, J. Kim, E. Hosono, H.-S. Zhou, T. Kudo, I. Honma, Nano Lett. 8 (2008) 2277–2282.
[8] D.Y. Pan, S. Wang, B. Zhao, M.H. Wu, H.J. Zhang, Y. Wang, Z. Jiao, Chem. Mater. 21 (2009) 3136–3142.
[9] G.X. Wang, X.P. Shen, J. Yao, J. Park, Carbon 47 (2009) 2049–2053.
[10] Y.J. Mai, X.L. Wang, J.Y. Xiang, Y.Q. Qiao, D. Zhang, C.D. Gu, J.P. Tu, Electrochim. Acta 56 (2011) 2306–2311.
[11] H. Kim, D.-H. Seo, S.-W. Kim, J. Kim, K. Kang, Carbon 49 (2011) 326–332.
[12] P.C. Lian, X.F. Zhu, S.Z. Liang, Z. Li, W.S. Yang, H.H. Wang, Electrochim. Acta 55 (2010) 3909–3914.
[13] G.X. Wang, B. Wang, X.L. Wang, J. Park, S.X. Dou, H. Ahn, K. Kim, J. Mater. Chem. 19 (2009) 8378–8384.
[14] Q. Zhang, S. D'Astorg, P. Xiao, X. Zhang, L. Lu, J. Power Sources 195 (2010) 2914–2917.

[15] J.Y. Xiang, J.P. Tu, J. Zhang, J. Zhong, D. Zhang, J.P. Cheng, Electrochem. Commun. 12 (2010) 1103–1107.
[16] U. Kasavajjula, C.S. Wang, A.J. Appleby, J. Power Sources 163 (2007) 1003–1039.
[17] S. Yoon, H. Kim, S.M. Oh, J. Power Sources 94 (2001) 68–73.
[18] S.S. Zhang, K. Xu, T.R. Jow, Electrochem. Commun. 5 (2003) 979–982.
[19] I.R.M. Kottegoda, Y. Kadoma, H. Ikuta, Y. Uchimoto, M. Wakihara, Electrochem. Solid State Lett. 5 (2002) A275–A278.
[20] S. Komaba, M. Watanabe, H. Groult, N. Kumagai, Carbon 46 (2008) 1184–1193.
[21] X.Y. Wang, X.F. Zhou, K. Yao, J.G. Zhang, Z.P. Liu, Carbon 49 (2011) 133–139.
[22] D.A.C. Brownson, D.K. Kampouris, C.E. Banks, J. Power Sources 196 (2011) 4873–4885.
[23] X.J. Zhu, Y.W. Zhu, S. Murali, M.D. Stoller, R.S. Ruoff, J. Power Sources 196 (2011) 6473–6477.
[24] Z.-S. Wu, W. Ren, L. Wen, L. Gao, J. Zhao, Z. Chen, G. Zhou, F. Li, H.-M. Cheng, ACS Nano 4 (2010) 3187–3194.
[25] H.F. Xiang, K. Zhang, G. Ji, J.Y. Lee, C.J. Zou, X.D. Chen, J.S. Wu, Carbon 49 (2011) 1787–1796.
[26] D.C. Marcano, D.V. Kosynkin, J.M. Berlin, A. Sinitskii, Z. Sun, A. Slesarev, L.B. Alemany, W. Lu, J.M. Tour, ACS Nano 4 (2010) 4806–4814.
[27] Y.J. Mai, J.P. Tu, X.H. Xia, C.D. Gu, X.L. Wang, J. Power Sources 196 (2011) 6388–6393.
[28] H.A. Becerril, J. Mao, Z. Liu, R.M. Stoltenberg, Z. Bao, Y. Chen, ACS Nano 2 (2008) 463–470.
[29] D. Zhan, Z.H. Ni, W. Chen, L. Sun, Z.Q. Luo, L.F. Lai, T. Yu, A.T.S. Wee, Z.X. Shen, Carbon 49 (2011) 1362–1366.
[30] D. Pacilé, J.C. Meyer, A. Fraile Rodríguez, M. Papagno, C. Gómez-Navarro, R.S. Sundaram, M. Burghard, K. Kern, C. Carbone, U. Kaiser, Carbon 49 (2011) 966–972.
[31] C. Goïmez-Navarro, J.C. Meyer, R.S. Sundaram, A. Chuvilin, S. Kurasch, M. Burghard, K. Kern, U. Kaiser, Nano Lett. 10 (2010) 1144–1148.
[32] X.R. Wang, S.M. Tabakman, H.J. Dai, J. Am. Chem. Soc. 130 (2008) 8152–8153.
[33] F. Béguin, F. Chevallier, C. Vix-Guterl, S. Saadallah, V. Bertagna, J.N. Rouzaud, E. Frackowiak, Carbon 43 (2005) 2160–2167.
[34] Y.P. Wu, C.Y. Jiang, C.R. Wan, E. Tsuchida, Electrochem. Commun. 2 (2000) 626–629.
[35] Y.H. Liu, J.S. Xue, T. Zheng, J.R. Dahn, Carbon 34 (1996) 193–200.
[36] J.R. Dahn, T. Zheng, Y. Liu, J.S. Xue, Science 270 (1995) 590–593.
[37] S.B. Yang, X.L. Feng, L.J. Zhi, Q.A. Cao, J. Maier, K. Mullen, Adv. Mater. 22 (2010) 838–842.
[38] A.V. Murugan, T. Muraliganth, A. Manthiram, Chem. Mater. 21 (2009) 5004–5006.
[39] J. Yao, X.P. Shen, B. Wang, H.K. Liu, G.X. Wang, Electrochem. Commun. 11 (2009) 1849–1852.
[40] J.Z. Wang, C. Zhong, S.-L. Chou, H.K. Liu, Electrochem. Commun. 12 (2010) 1467–1470.
[41] B. Wang, X.L. Wu, C.Y. Shu, Y.G. Guo, C.R. Wang, J. Mater. Chem. 20 (2010) 10661–10664.
[42] D. Aurbach, I. Weissman, A. Schechter, H. Cohen, Langmuir 12 (1996) 3991–4007.
[43] M.D. Levi, D. Aurbach, J. Phys. Chem. B 101 (1997) 4630–4640.
[44] C. Lai, H.Z. Zhang, G.R. Li, X.P. Gao, J. Power Sources 196 (2011) 4735–4740.
[45] M.D. Levi, D. Aurbach, J. Phys. Chem. B 101 (1997) 4641–4647.
[46] M.V. Reddy, T. Yu, C.H. Sow, Z.X. Shen, C.T. Lim, G.V. Subba Rao, B.V.R. Chowdari, Adv. Funct. Mater. 17 (2007) 2792–2799.